RSC Advances




ROYAL SOCIETY OF CHEMISTRY

www.rsc.org/advances

# A General Electrodeposition-Based Method for In-Situ Construction of Resistive-Type Semiconductor Film Gas-Sensor with Excellent Sensing Performance

Zizhao Pan[a], Fengqiang Sun[*a, b, c], Shipu Xu[a], Jinfeng Long[a], Ying Chen[a] and Zefeng Zhuang[a]

[a]School of Chemistry and Environment, South China Normal University, Guangzhou 510006, P. R. China.

[b]Key Laboratory of Theoretical Chemistry of Environment, Ministry of Education, South China Normal University, P. R. China.

[c]Guangzhou Key Laboratory of Materials for Energy Conversion and Storage, P. R. China.

* Corresponding author: Fengqiang Sun, e-mail: fqsun@scnu.edu.cn; Tel & Fax: 86-20-39310187.

**Abstract**

For construction of a resistive-type gas-sensor, a sensing film usually requires to be fabricated on a non-conductive substrate. Subjecting to the substrate, in-situ construction of a sensor by the electrodeposition method is impossible and there has been no related report. Herein, taking the in-situ construction of $SnO_2$ film sensor as an example, a novel electrodeposition-based method was introduced. A conductive graphite coating was firstly fabricated on the non-conductive substrate for the implementation of the electrodeposition, and then a calcining process was employed. The conductive pristine graphite coating was found became non-conductive after calcined more than 70 min at 500 ℃, resulting in that the final electrodeposited film could work as a sensing film. Some important parameters related to the sensing performances, including the formation, the conductivity, the electrodeposition time, the calcining time and the working temperature were systematically studied. Under the optimal conditions, the $SnO_2$ film sensor exhibited high sensitivity, fast response and recovery, and long-term stability in detecting ethanol gas with concentration of 1-100 ppm. The electrodeposition-based method was reproductive, mass-productive and general. It was therefore practical and promising in construction of various semiconductor film sensors.

**Keywords:** electrodeposition, graphite coating, $SnO_2$, gas sensor

## Introduction

The resistive-type gas sensor represents a kind of conventional device for the detection of flammable and noxious environmental gases. It is composed of a non-conductive ceramic substrate, two electrodes on the ends of the substrate and a sensing film connecting the two electrodes. Coating of the sensing film onto the substrate is essential and even decisive for obtaining a sensor with excellent sensitivity, stability and/or reproducibility.

Generally, the sensor film is fabricated by three steps [1-3], i. e. synthesizing powder-like sensing materials with various methods, blending powders with specific liquids into pastes and then coating pastes onto substrates, which is widely employed in studies focused on the sensing property of a material. However, in addition to the fussy manipulations, the particles in the coated film usually physically contact each other and their morphologies are easily destroyed during the coating process, inherently resulting in the instability, the undefined sensitivity and the reproducibility of the final sensor. Some in-situ methods, like chemical vapor deposition (CVD) [4, 5], physical vapor deposition (PVD) [6], and electrospinning process [7, 8] can be used to directly grow sensing film on the corresponding substrates and effectively overcome the drawbacks of the three-step method, but they are restricted to the fabrication of film on the flat substrate and must require the sophisticated equipment, limiting their more widely applications. Recently, the monolayer colloidal crystal template method developed by our groups can fabricate the ordered porous sensing film directly on various substrates and because of the assistance of templates the reproductive construction of sensors is also feasible [9-11]. However, the method still locks into obtaining a large area ideal template with little or without defect and sometimes layer-by-layer

manipulations must be carried out to improve the conductivity of a film, limiting the mass-production of sensors.

Electrodeposition, a traditional method for fabricating films on conductive solid substrates, has many advantages, such as requiring simple apparatus, easy manipulation, strong controllability, low cost and mass production. Till now, electrodepositions of nearly all semiconductor materials suitably used in gas-sensor have been achieved. These are obviously beneficial to the construction, performance-improvement and practicality of gas-sensors. However, because the substrate of a gas-sensor is non-conductive, direct electrodeposition of a sensing film on such a substrate is completely impossible. Alternatively, in several reports [12-14], sensing materials had to be electrodeposited on conductive substrates first and then peeled off, transferred on special substrates (e.g. polystyrene film) and processed with additional electrodes for construction of specific sensors. The subsequent manipulations were difficult and not suitable for most sensing materials in addition to that they could cause more or less mechanical damages to the materials. The application of the electrodeposition method in construction of a gas-sensor device still suffers from severe limitations and the advantages of electrodeposition cannot be fully embodied. Growth of sensing materials on available ordinary substrates directly used in gas-sensor is obviously necessary, but none has tried to do so because of the limitation of the non-conductivity of the substrate.

Herein, a new process for construction of the gas-sensor based on the electrodeposition is introduced. A ceramic tube widely used in the field of gas-sensor was chosen as the substrate. In order to make the substrate conductive, the surface of the substrate was coated with a graphite film, which was a key step. And then the electrodeposition of semiconductor could

be favorably carried out on the substrate. After a subsequent calcination process, the graphite layer was found had a particular character, i. e., its conductivity would be significantly decreased and finally disappear, which guaranteed the electrodeposited film could directly work as a sensing film. Thus, the construction of a sensor by the electrodeposition would be very easy, and every available inorganic semiconductor sensor could be obtained by this method. For more clearly explaining the process and the sensing performances of the as-prepared sensor, $SnO_2$, the most widely used material in gas-sensor was chosen as an example.

## Experimental

### Construction of the gas-sensor

A commercially applied ceramic tube (Scheme 1a) with outer diameter of 2 mm and length of 5 mm was employed as the substrate. It contains two conductive gold films around the ends, electrode wires welded on the gold films and the naked non-conductive ceramic surface (Scheme 1a). Before used, it was ultrasonically cleaned sequentially in acetone and in ethanol, and dried. An ordinary cuboid graphite block was then repeatedly uniformly scraped the surface of the tube to acquire a conductive graphite coating connecting the gold films on the ends (Scheme 1b). The resistance was controlled at ~80Ω. Subsequently, the electrode wires on the two ends of the tube were connected with the cathode of a Galvanostatic instrument (Scheme 1c). And then the tube was immersed into 30 mL electrolytic solution in an electrolytic cell with a graphite electrode as counter electrode. Typically, for fabrication of $SnO_2$ film, the electrolytic solution was composed of 0.02 M $SnSO_4$, 0.1 M $NaNO_3$ and 0.075

$HNO_3$; the electrodeposition was carried out at 0.8 mA; 90 min later, the electrodeposition was stopped. The tube was then taken out, washed with deionized water, dried at room temperature and calcined at 500 ℃ to increase the resistance of the graphite coating and promote the formation of $SnO_2$ film. After 100 min, heat treatment was stopped and a $SnO_2$/graphite hybrid film gas-sensor was finally obtained (Scheme 1d). Subsequently, a spring-like nickel-chromed (Ni-Cr) alloy heating wire was crossed through the tube. The heating wire and the electrodes of the ceramic tube were then welded on a specific support used in a gas-sensing test system (Scheme 1e). The as-constructed gas-sensor could work. Other semiconductor/graphite sensors could be also constructed by the similar process.

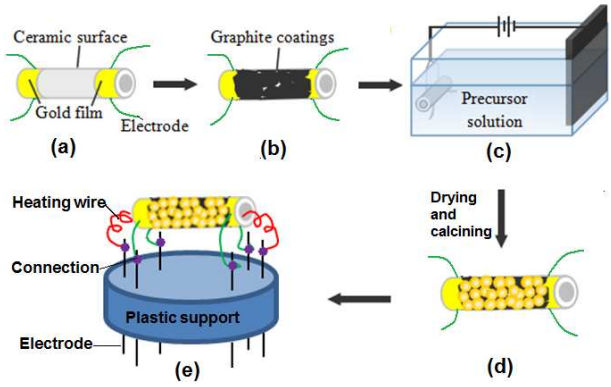


**Scheme 1** Fabrication process of the semiconductor/graphite gas-sensor based on the electrodeposition method. (a) Schematic of the ceramic tube used as the substrate; (b) tube covered with the graphite coating; (c) electrodeposition of semiconductor on the tube; (d) semiconductor film on the graphite-covered tube; (e) tube connected on a specific support.

## Gas-sensing test

The gas sensing test was operated on a WS-30A system (Weisheng Instruments Co., Zhengzhou, China). The detection of ethanol gas was chosen as an example to evaluate the

performance of the as-constructed sensors. A stationary state gas distribution method was carried out for gas response testing. The working temperature of the sensors was adjusted by varying the heating voltage at the Cr-Ni wire and monitored with a thermometer. The ethanol gas to be detected was injected into a test chamber and mixed with air. The conductivity (or resistance) of the sensor would be changed. After it was stabilized, the chamber was opened and the ethanol gas was removed. The conductivity would be recovered. The same procedure was followed for the recycling test.

**Characterizations**

The morphologies of graphite coating and $SnO_2$/graphite hybrid film on the ceramic tubes were examined by scanning electron microscopy (SEM, Shimadzu SS-550 and Quanta 250 FEG). The compositions were characterized by X-ray powder diffraction (XRD, D/max2200, with Cu Kαradiation). Samples for the XRD measurements were prepared on the frosted glass substrates under the same conditions as those for preparation on the ceramic tubes.

**Results and discussion**

**Character of the graphite coating**

Figure 1a shows the morphology of a pure pristine graphite coating fabricated by scraping the surface of the ceramic tube with a graphite block. It uniformly covered the whole surface of the ceramic tube and was composed of closely contacted graphite sheets and indistinguishable carbon fine particles. Although there were some micro-cracks, the coating still had very high conductivity. The resistance was around 80 Ω, approximatively a liminal

value, which was easily obtained by controlling the scraping time. Different from the graphite block with high thermal stability, the carbon fine particles and the edges of graphite sheets in the coating should have higher surface energy because of their super small sizes, according to the general physicochemical theory. As a result, when this coating was calcined at a high temperature in air, these fine particles and edges had higher reactive activities with oxygen and were preferentially removed away. The thermogravimetric curve of the corresponding graphite powder in the simulate air showed the weight loss continually increased when the temperature was increased (Figure 1b). In the range of 200~500 $^{o}$C, the loss should be attributed to the removals of fine carbon particles and the edges of the graphite sheets. Higher than 500 $^{o}$C, all graphite sheets would be also removed quickly. Here, the temperature of 500 $^{o}$C was optimized to calcine the graphite coating. Figure 1c shows the morphology of the graphite coating after calcined 100 min. Due to the loss of partial carbon and the expanding-shrinking action of graphite sheets in the heating-cooling process, the coating became very loose. The graphite sheets with irregular edges and lots of pores among sheets could be clearly identified. The conductivity of the graphite coating was thereby drastically decreased and varied with the calcining time. As shown in Figure 1d, as time increased to 70 min, the resistance of the coating gradually increased from 0.1 to 1346 KΩ. After that, the resistance was too high to be measured and the coating was thought became non-conductive. These characters are obviously beneficial to the electrodeposition construction of a semiconductor gas-sensor on the graphite coating. We can electrodeposit a semiconductor film on the pristine graphite coating covered substrate (without heated) and then decreased the conductivity of the coating by a calcining process to make the final semiconductor film lie on

a non-conductive support.

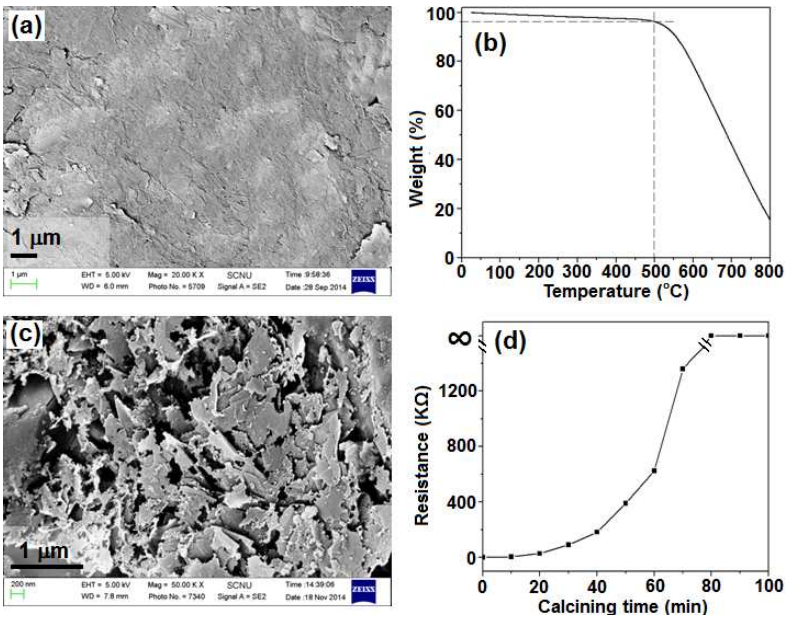


**Figure 1** Characters of the graphite coating. (a) SEM image of the pristine graphite coating; (b) thermogravimetric curve of the graphite powder; (c) SEM image of the graphite coating calcined 100 min at 500 °C; (d) Variation of the resistance of the coating with increase of the calcining time.

**The electrodeposited film on the graphite coating**

Figure 2a shows the morphology of the electrodeposited film on the pristine graphite coating covered on the ceramic tube after deposition of 90 min and before calcined. The film was composed of closely packed spherical particles with the size of 80~200 nm. Because of the influence of the bottom graphite coating, some cracks could be generated during the growth of the film. In the XRD pattern (Figure 2b-①) of the hybrid film (composed of the bottom graphite coating and the upper electrodeposited film), only a peak at ~26° was found and it should be attributed to the carbon (002) plane, explaining the electrodeposited particle

film was amorphous. After calcined 100 min at 500 $^{o}$C, the amorphous substance was transformed into crystalline $SnO_2$. (110), (101) and (211) planes of $SnO_2$ were clearly displayed in the corresponding XRD pattern (JCPDS no. 41-1445) (Figure 2b-②). The peak of graphite could be still discerned. The morphology of the calcined sample was shown in Figure 2c. The shapes and sizes of the particles remained approximately consistent with those before calcined. However, the cracks had been multiplied and enlarged, which divided the film into some patches in certain areas. Through the cracks (inset of Figure 1c), the graphite sheets could be found and they connected the adjacent $SnO_2$ particle film patches. Notably, during the calcining process, the resistance of the hybrid film experienced a regular variation (Figure 2d). It first gradually increased from 0.14 KΩ (resistance of the hybrid film before calcined) to 680 KΩ as the calcining time increased to 100 min and then could nearly remain unchanged when the calcination continued.

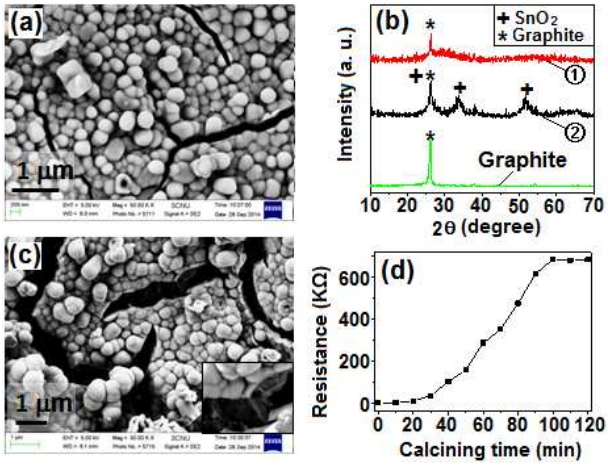


**Figure 2** Characterizations of the electrodeposited film on the graphite coating. (a)SEM image of the film before calcined; (b) XRD pattern of the film before (①) and after (②) calcined 100 min; (c) SEM image of the film calcined 100 min; (d) variation of resistance of the film with the calcining time. The calcining temperature was controlled at 500 $^{o}$C

**Formation and conductive mechanism of the film on the graphite coating**

During the electrodeposition process in the mixed solution of $SnSO_4$, $NaNO_3$ and $HNO_3$ at room-temperature, on the cathode electrode surface (graphite coating), two half reactions would occur as follows [15-17]:

$$NO_3^- + H_2O + 2e^- \longrightarrow NO_2^- + 2OH^- \quad (1)$$

$$NO_3^- + 7H_2O + 8e^- \longrightarrow NH_4^+ + 10OH^- \quad (2)$$

Once $OH^-$ ions formed on the graphite coating, they would then immediately reacted with $Sn^{2+}$ ions to form $Sn(OH)_2$:

$$Sn^{2+} + 2OH^- \longrightarrow Sn(OH)_2 \downarrow \quad (3)$$

In the electrolyte exposed in air, partial $Sn^{2+}$ ions might be oxidized into $Sn^{4+}$ ions, and these ions still reacted with $OH^-$ ions to produce $Sn(OH)_4$. Because the surface of the graphite coating was nearly homogenous, plus the corresponding reactions were very quick, the as-formed tin hydroxide particles showed spherical shape and amorphous state (Figure 2b). In the subsequent heat-treatment in air at 500 $^oC$, tin hydroxides would be decomposed and oxidized to generate crystalline $SnO_2$. At the same time, the graphite coating in the bottom would be partially oxidized and expanded. Because of the difference in expansion coefficients between graphite and the tin-contained compounds (i. e. tin hydroxides and $SnO_2$), the electrodeposited film naturally generated many cracks. Accompanying these chemical changes and physical actions, the conductivity of the heated film would be decreased gradually until it reached a stable state, as shown in Figure 2d.

The conductivity mechanism was suggested as follows. Based on the electrodeposition principle, the obtained tin-contained compound film must be always closely adhered to the

graphite coating even though they were heated at a high temperature and generated many cracks, as shown in Schemes 2a and 2b. Once a voltage was applied on the electrodes on the two ends of the ceramic tube, the bottom graphite coating and the upper tin-contained compound film could form a circuit (Schemes 2a1 and 2b1). Because of the difference between the two films in resistance, the intensity of current allocated in them would be different [18]. Before calcined, the electrodeposited amorphous tin hydroxides were non-conductive and had the super high resistance, but the pristine graphite coating was a good conductor with very low resistance, resulting in that the current only passed through the graphite coating (Scheme 2a1). As the calcining time increased, tin hydroxides were gradually transformed into crystalline $SnO_2$ with decreased resistance and increased conductivity, while the resistance of the graphite coating was always increased (as shown in Figure 1d). The current would be thereby allowed to pass through the $SnO_2$ layer. After calcined 100 min, the bottom graphite layer had been changed non-conductive as a whole, but in the local areas composed of one or several closely overlying graphite sheets could still have good conductivity and act as conductive wires to connect the cracks in the upper $SnO_2$ layer (as shown in Figure 2c). Due to the deletion of the conductivity of the graphite layer and the formation of the stable $SnO_2$ layer, the resistance of the hybrid film kept stable and the current only passed through the $SnO_2$ layer (Scheme 2c). This was essential for the $SnO_2$ film working as a resistance-type gas-sensing film.

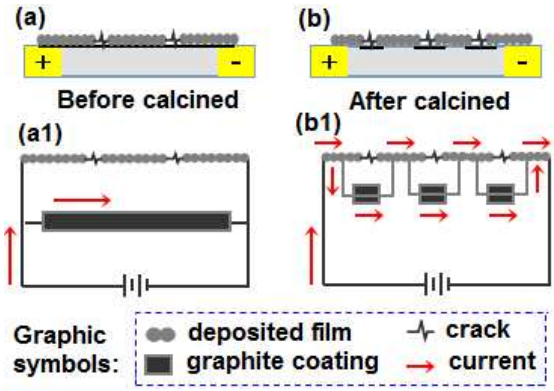


**Scheme 2** Schematic illustration of state of the electrodeposited film and the graphite coating. (a) and (b) show the state of the hybrid film before and after calcined, respectively; (a1) and (b1) show the circuit and the current flowing in the hybrid film corresponding to a and b, respectively, after a voltage applied on the two ends of the ceramic tube.

**Gas-sensitivity of the film sensor**

The ceramic tube covered with the $SnO_2$/graphite hybrid film (heated 100 min at 450 $^oC$) could be directly constructed into a kind of resistive type gas sensor (Figure 3a) used for the detection of ethanol gas in the surroundings. For a practical gas-sensor, it should work at a suitable temperature to quickly response to the ethanol gas, exhibit the highest sensitivity and quickly recover. Figure 3b shows the response of the sensor to 50 ppm ethanol gas at different working temperatures. The gas sensitivity is defined as $S= R_{air}/R_{gas}$, where $R_{air}$ and $R_{gas}$ are the resistances of the sensor in the air and the air mixed with ethanol gas, respectively [19]. The response time is defined as the time required for reaching 90% of the equilibrium value; the recovery time is defined as the time taken for the sensor output to be decreased to 10% of its steady value after the gas was removed. When the temperature was lower than 100 °C, no signal could be detected. At 100 °C, a sensitivity of 2.0 was obtained (Figure 3c), the response

time was calculated as 35 s (inset of Figure 3b), but the sensor couldn't be completely recovered. As the temperature increased to 160 °C, the sensitivity gradually increased to the maximum, 8.9; both of the response and the recovery time decreased to 8 s. In the range of 160 ~ 240 °C, the sensitivity, the response time and the recovery time were nearly unvaried. When the temperature was higher than 240 °C, the sensitivity decreased with the increase of the temperature; the response and the recovery time kept consistent. Obviously, the sensor could work in a wide range of temperature, exhibiting the optimal excellent performances. For energy-saving, the working temperature was optimized as 160 °C. At this temperature, the sensor could be employed to effectively detect different concentrations of ethanol gas mixed in air (Figure 3d). The limit concentration of the detectable ethanol gas was as low as 1 ppm. The sensitivity noticeably increased with the increase of the gas concentration (Figure 3e). When the concentration increased from 1 to 100 ppm, the sensitivity gradually increased from 2.2 to 10.4. The response time and the corresponding recovery time were always limited in the range of 7~9 s.

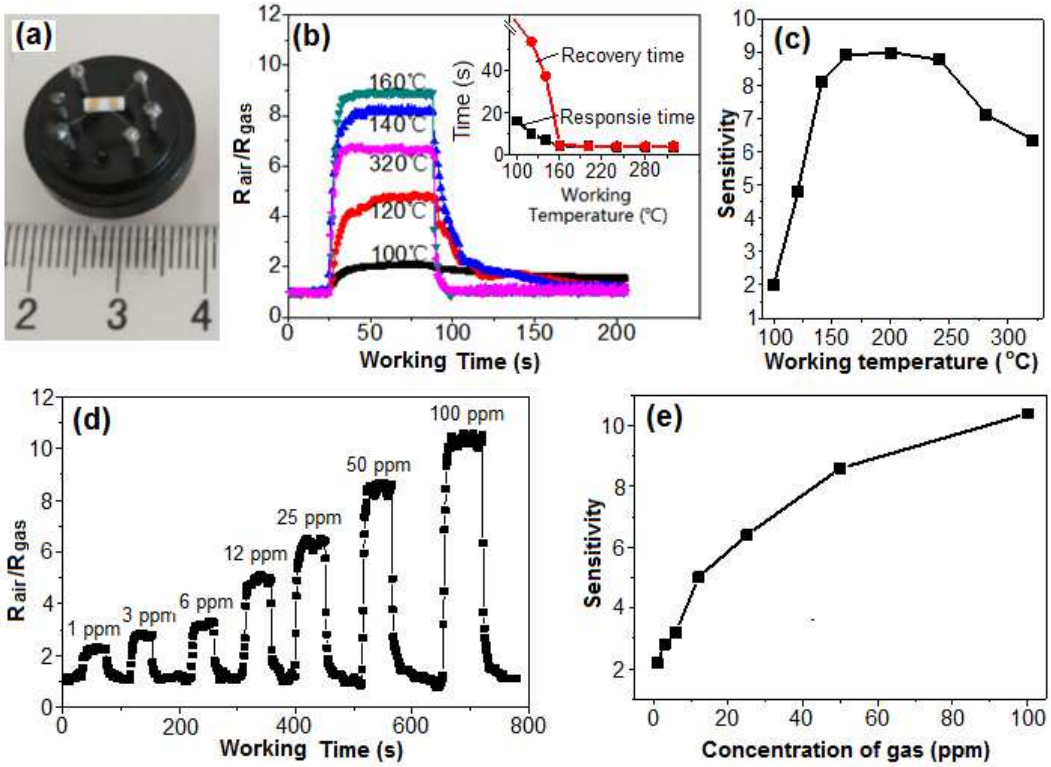


**Figure 3** (a) a photo of the $SnO_2$/graphite hybrid film sensor; (b) and (c) response and sensitivity of the sensor in detecting 50 ppm ethanol gas at different working temperature; the inset of (b) shows the corresponding response and recovery time; (d) and (e) response and sensitivity of the sensor in detecting different concentration of ethanol gas at 160 °C.

**Sensing mechanism and influential facts on the sensitivity**

Generally, for the n-type $SnO_2$ semiconductor, when it is used in gas-sensor and exposed in air, $O_2$ molecules will be chemisorbed and capture some electrons of $SnO_2$ to be changed into $O_2^-$, $O^-$ and $O^{2-}$ on the sensing body surfaces [20, 21]. After the reducing gas (e.g., ethanol gas) is introduced, some oxygen species will be reduced and removed from the surfaces, and the captured electrons will be released to pour back to $SnO_2$, resulting in the variation of the resistance of $SnO_2$ and the exhibition of sensitivity. For the $SnO_2$/graphite hybrid film

reported here, because the pure graphite film (whether heated or not) had no response to ethanol gas (not shown here), the surface area of the $SnO_2$ film exposed in atmosphere and the ratio of the electric current passing through the $SnO_2$ film would be decisive for the final sensitivity of the hybrid film. It was thereby easily deduced the electrodeposition time and the calcining time in the fabrication process should put essential impacts on the sensitivity of the final film.

Figure 4a shows the response of the films obtained from different electrodeposition time to 50 ppm ethanol gas. All films had been calcined 100 min at 500 °C and the bottom graphite coating should be non-conductive. In a short electrodeposition time, for example, in 15 min, the obtained film constituted by $SnO_2$ particles with smaller sizes should be thinner and be easier to be broken to generate more and bigger cracks in per unit area during the heating process, resulting in the less exposed surface area of $SnO_2$ film and the lower sensitivity (3.1). With the increase of the electrodeposition time, the particles became bigger and the final $SnO_2$ film was densified, thickened and strengthened. These could reduce the number and the size of cracks in the film, increasing the exposed surface area and the sensitivity of $SnO_2$ film. After electrodeposition of 90 min, the resulted $SnO_2$ film could have the maximum surface area and the maximum sensitivity (8.9). Continually increasing the electrodeposition time, the thickness of the film might be increased but the surface area couldn't be changed, so that the sensitivity kept consistent.

Taking the sample from 90 min electrodeposition as an optimal example, the effect of the calcining time on the sensitivity of the hybrid film was analyzed. Figure 4b shows the sensitivity of the film varied with the calcining time in detecting 50 ppm ethanol gas. Before

calcined, the electric current only passed through the graphite layer and there was no $SnO_2$ particle in the electrodeposited layer, so the hybrid film had no response. Once the calcination at 500 °C began, the conductivity of the graphite layer gradually decreased but that of the electrodeposited layer increased because of the continuous generation of $SnO_2$ particles, resulting in increase of the ratio of current allocated in the electrodeposited layer when the sensor worked. The electric signal caused by the variation of the resistance of the film would be more easily detected and showed the higher variations, plus the total surface area of $SnO_2$ particles increased, leading to the gradual increase of the sensitivity until the calcining time reached 80 min. Since then, the graphite layer became non-conductive, there was no new $SnO_2$ particle generated and the sensitivity couldn't vary with the calcining time.

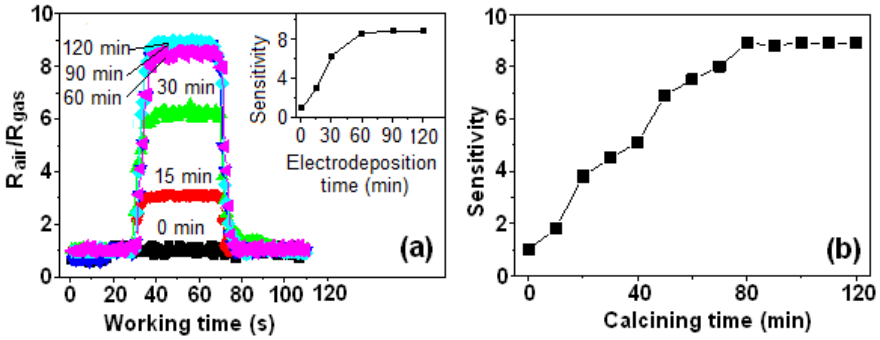


**Figure 4** Effects of electrodeposition time and calcining time in the fabrication process of the sensor on the sensing performance. (a) Response of sensors from different electrodeposition time to 50 ppm ethanol gas; (b) the sensitivity of sensors from different calcining time in detecting 50 ppm ethanol gas.

Further, it should be noted, the final film was composed of spherical particles and there were many naked spherical surfaces (Figure 2c). This increased the total surface area of the film, enhanced the adsorption for oxygen negative ions and increased the sensitivity. Besides, the grain boundary in the film could also adsorb oxygen negative ions and put an impact on

the sensing performances of the film [22]. As we know, in the electrodeposition process, adjacent particles with different crystallization orientations can gradually contact and cross each other as they grow up, resulting in the formation of chemical bonding and grain boundaries among them; in the subsequent calcining processes at high temperature, atoms are more active and easier to diffuse, and the connections among the particles is enhanced. With the increase of the electrodeposition time and the calcining time, the total number of grain boundary would be increased until the film reached the steady state. Thereby, the final $SnO_2$ film patch here could be considered as a poly-crystal with many grain boundaries. For $SnO_2$ gas-sensor, two different conduction mechanisms, grain boundary conduction and neck conduction, had been proposed [23, 24], in addition to the surface conduction mechanism. Here, the particles had grown together and most necks were removed. Grain boundary conduction would play an essential role for the film [25]. Atoms in the grain boundary had higher activity than those in other regions and easily adsorbed more oxygen negative ions in air to build potential barriers at a lower temperature (e. g. 160 $^{o}$C). After the oxygen negative ions reacted with the introduced ethanol gas, a high conductivity (/resistance) change (i. e. sensitivity) would be exhibited. Still based on the electrodeposition mechanism, more grain boundaries should locate near the surface of the film. Meanwhile, grain boundaries buried in the bulk region were believed to be chemically inactive due to the dense morphology of the thin film [26]. These could be further confirmed by that the sensitivity of the film was nearly unvaried with electrodeposition time once the time was longer than 90 min (Figure 4). The adsorption/desorption of oxygen negative ions mainly occurred near the surface of the film, resulting in the quick response and quick recovery of the film sensor. Additionally, the close

contact between the film and the substrate could allow a steady current to pass through the film and further enhance the sensing performances of the sensor. The comparison of sensor responses of some pure $SnO_2$ gas sensors for ethanol sensing was summarized in Table 1. It was found the present sensor exhibited better sensing properties including the optimized working temperature, the sensitivity and the response/recovery time.

**Table 1 Comparison of sensing characteristics of pure $SnO_2$ gas sensors fabricated with different methods**

| Methods | Working temperature (℃) | Sensitivity (gas concentration) | Response/ recovery time (s) | Ref. |
|---|---|---|---|---|
| **In-situ electrodeposition** | 160 | 8.9 (50 ppm) | 8/8 | This work |
| **Molecular beam epitaxy** | 400 | 2.8 (100 ppm) | 80/320 | 27 |
| **Pulsed laser deposition** | 250 | 7 (60 ppm) | 8/20 | 28 |
| **Sputtering method** | 350 | 2.5 (50 ppm) | -/- | 29 |
| **Photochemical deposition** | 260 | 4.6 (100 ppm) | 10/8 | 10 |
| **Thermal evaporation** | 350 | 3.78 (50 ppm) | -/- | 30 |
| **Sol-gel template method** | 200 | 3.5 (50 ppm) | -/- | 31 |
| **Manually coating** | 300 | 7 (50 ppm) | 7/20 | 32 |
| **Sol-gel method** | 250 | 3.2 (150 ppm) | -/- | 33 |
| **Spin coating** | 200 | 6.2 (400 ppm) | 170/- | 34 |

**Practicality of the electrodeposition method in fabrication of gas-sensor**

In the fabrication process, the electrodeposition time and the calcining time were easily controlled in a wide range to let the sensing performance of $SnO_2$/graphite hybrid film reach the steady limit state, which was beneficial to the reproduction of sensors with uniform performance. As shown in Figure 6a, the sensitivity of four sensors fabricated one by one under the same conditions was nearly kept consistent in detecting 50 ppm ethanol gas. Moreover, because of the controllability of the fabrication parameters, mass production of sensors was also feasible. For mass production, during the electrodeposition process, several

ceramic tubes could be concurrently connected (in parallel) to the cathode of the power source to obtain the uniform films and then they experienced the same heat-treatments. Different sensors fabricated for one time could exhibit approximately the same sensing performance (Figure 5b). More interestingly, the sensor also showed super high stability (Figure 4d). After the sensor experienced more than 100 tests and placed in ordinary surroundings for more than 9 months without any protection, it still exhibited nearly the same sensitivity as that when it was first used in detection of 50 ppm ethanol gas. Thus, the sensor may be reused continuously. Humidity and $CO_2$ gas are important factors that might affect the gas-sensing properties of a semiconductor metal oxide. The $SnO_2$ film sensor had been thus investigated for detecting 50 ppm ethanol gas under different relative humidities and in the mixed gases containing different concentration of $CO_2$ gas, respectively, as shown in Figures 5d and 5e. As the relative humidity increased from 50% to 90%, the sensitivity exhibited a decrease of ~6.5%; in the mixed gas containing $CO_2$, as the concentration of the additionally introduced $CO_2$ increased to 3 vol.%, the sensitivity exhibited a decrease of ~2.5%. These slight variations in sensitivity and the nearly unvaried response/recovery time demonstrated the humidity and $CO_2$ gas in air had little influence on the sensor. In addition, the method was general in fabrication of semiconductor film gas-sensors on the substrate covered with graphite coating. By this method, ZnO, $Fe_2O_3$, CuO and NiO film sensors had been also fabricated according to the reported electrodeposition process [35-39]. They could response to ethanol gas too and exhibit a specific sensitivity, respectively (Figure 5f). For the p-type CuO and NiO film, their resistances decreased with the injection of reductive ethanol gas and their sensitivity were defined as $S=R_{gas}/R_{air}$. Finally, it should be noted the electrodeposition

method is flexible and many strategies, for example, addition of suitable surfactants in the electrolyte, use of templates, layer-by-layer construction and co-deposition, can be employed to control the morphology, the surface area or composition of the film, which implies there are infinite impossibilities in construction of excellent gas-sensors. Many studies on these are in progress.

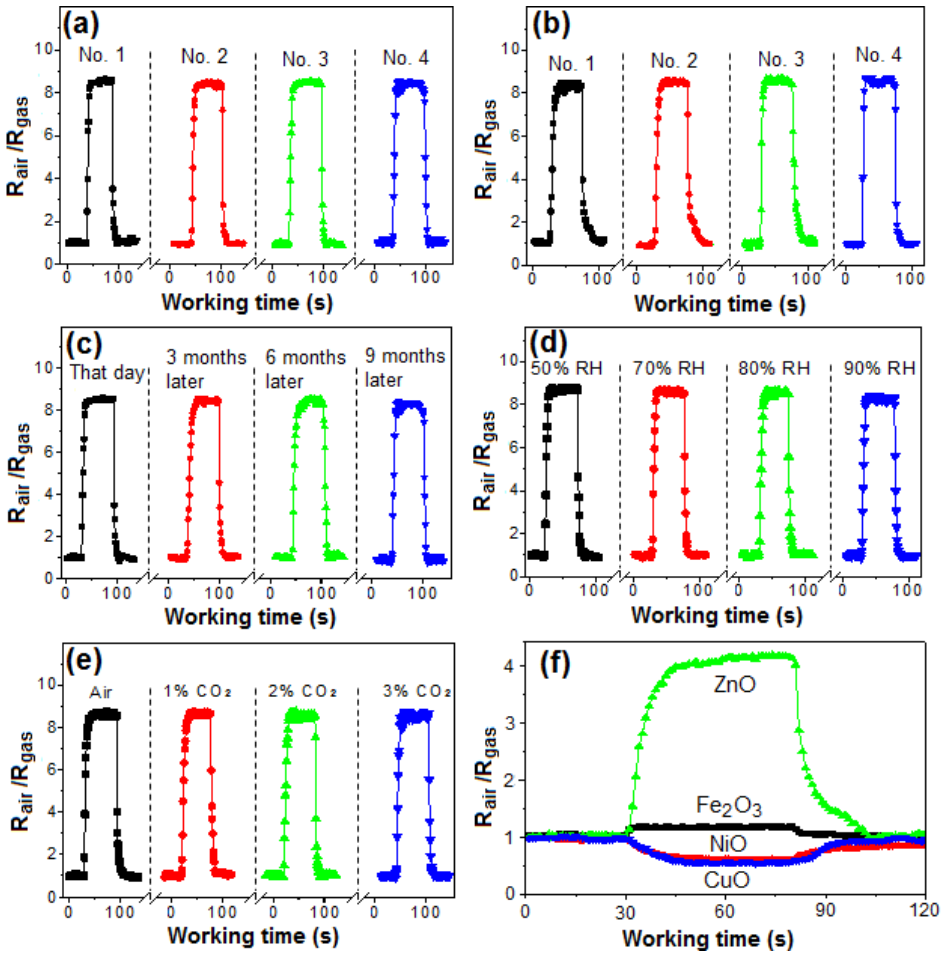


**Figure 5** (a) Responses of the reproduced sensors; (b) the mass-produced sensors; (c) a sensor after placed certain time in ordinary surroundings; (d) effect of humidity on the response of a sensor (RH represents the relative humidity); (e) effect of additionally introduced $CO_2$ gas on the response of a sensor; and (d) some other typical oxide sensors in detecting 50 ppm ethanol gas.

## Conclusions

In summary, based on an electrodeposition method and with the assistance of a calcining process, semiconductor film gas-sensors had been in-situ constructed on a non-conductive substrate covered with graphite coating. The pristine graphite coating had excellent conductivity and contributed to the implementation of the electrodeposition; after calcined, it became non-conductive as a whole and the semiconductor film could then work as a gas-sensor. For the obtained $SnO_2$ film sensor, it had been used in detecting ethanol gas with concentration of as low as 1 ppm, showing fast response and recovery, high sensitivity and long-term stability. Electrodeposition time and calcining time could put impacts on the sensing performance, but once they were controlled to higher than a specific value, the sensitivity of the film would always keep nearly constant. Due to the easy controllability, the fabrication method showed the extraordinary practicality and could be used in the reproduction and the mass-production of a semiconductor film sensor. The method is also general. In addition to the metallic oxide (e. g. $SnO_2$, ZnO, $Fe_2O_3$, CuO and NiO) film sensors mentioned here, in theory, any semiconductor film (with good thermal stability) sensor could be constructed.

## Acknowledgements

This work was co-supported by the Research Project of Chinese Ministry of Education (No. 213029A), the National Natural Science Foundation of China (No. 31071057), the Natural Science Foundation of Guangdong Province (Nos. 10351063101000001) and the Special funds for Discipline Construction in Guangdong Province (No. 2013KJCX0057).

**Notes and references**

[1] G. Neri, S. G. Leonardi, M. Latino, N. Donato, S. Baek, D. E. Conte, P. A. Russo and N. Pinna, *Sensor. Actuat. B- Chem.,* 2013, **179**, 61-68.

[2] L. H. Zhu, D. Z. Zhang, Y. Wang, C. H. Feng, J. R. Zhou, C. X. Liu, and S. P. Ruan, *RSC Adv.*, 2015, **5**, 28105-28110.

[3] S. Thirumalairajan, V. R. Mastelaro and C. A. Escanhoela, *ACS Appl. Mater. Interfaces*, 2014, **6**, 21739-21749.

[4] F. E. Annanouch, I. Gracia, E. Figueras, E. Llobet, C. Cane and S. Vallejos, *Sensor. Actuat. B-Chem.,* 2015, **216**, 374-383.

[5] Q. N. Abdullah, F. K. Yam, J. J. Hassan, C. W. Chin, Z. Hassan and M. Bououdina, *Int. J. Hydrogen Energ.,* 2013, **38**, 14085-14101.

[6] K. Lizuka, M. Kambara and T. Yoshida, *Sensor. Actuat. B-Chem.,* 2012, **173**, 455-461.

[7] O. Landau, A. Rothschild and E. Zussman, *Chem. Mater.,* 2009, **21**, 9-11.

[8] W. Tang and J. Wang, *J. Mater. Sci.,* 2015, **50**, 4209-4220.

[9] F. Q. Sun, W. P. Cai, Y. Li, L. C. Jia, and F. Lu, *Adv. Mater.,* 2005, **17**, 2872-2876.

[10] S. P. Xu, F. Q. Sun, F. L. Gu, Y. B. Zuo, L. H. Zhang, C. F. Fan, S. M. Yang, and W. S. Li, *ACS Appl. Mater. Interfaces,* 2014, **6**, 1251-1257.

[11] S. P. Xu, F. Q. Sun, S. M. Yang, Z. Z. Pan, J. F. Long and F. L. Gu, *Sci. Rep.* 2015, **5**, 8939

[12] A. Star, V. Joshi, S. Skarupo, D. Thomas and J. P. Gabriel, *J. Phys. Chem. B,* 2006, **110**, 21014-21020.

[13]D. Jung, M. Han and G. S. Lee, *Carbon,* 2014, **78**, 156 –163.

[14]M. Z. Atashbar and S. Singamaneni, *Sensor. Actuat. B- Chem.,* 2005, **111-112,** 13-21.

[15]S. T. Chang, I. C. Leu, M. H. Hon, *J. Cryst. Growth*, 2004, **273**, 195–202.

[16]X. P. Chen, J. Y. Liang, Z. T. Zhou, H. N. Duan, B. Q. Li, Q. M. Yang, *Mater. Res. Bull.,* 2010, **45**, 2006–2011.

[17]E. Hosono, S. Fujihara, H. Imai, I. Honma and H. Zhou, *Chem. Commun.,* 2005, 2609–2611.

[18]A. Tricoli and S. E. Pratsinis, *Nat. Nanotechnol.,* 2010, **5**, 54-60.

[19]X. Y. Lai, J. Li, B. A. Korgel, Z. H. Dong, Z. M. Li, F. B. Su, J. A. Du and D. Wang, *Angew. Chem.-Int. Edit.,* 2011, **50,** 2738-2741.

[20]G. H. Lu, L. E. Ocola and J. H. Chen, *Adv. Mater.,* 2009, **21**, 2487–2491.

[21]S. Mao, S. M Cui, G. H. Lu, K. H. Yu, Z. H. Wen, J. H. Chen, *J. Mater. Chem.,* 2012, **22**, 11009–11013.

[22]J. R. Huang, K. Yu, C. P. Gu, M. H. Zhai, Y. J. Wu, M. Yang, J. H. Liu, *Sensor. Actuat. B-Chem.*, 2010, **147**, 467 – 474.

[23]Z. H. Jin, H. J. Zhou, Z. L. Jin, R. F. Savinell, C. C.Liu, *Sensor. Actuat. B- Chem.* 1998, **52**, 188–194.

[24]Y. Liu, E. Koep, M.L. Liu, *Chem. Mater.,* 2005**, 17***,* 3997-4000.

[25]L.G. Teoh, Y.M. Hon, J. Shieh, W.H. Lai, M.H. Hon, *Sensor. Actuat. B- Chem.*, 2003, 96, 219–225.

[26]S. W. Lee, P. P. Tsai, H. Chen, *Sensor. Actuat. B- Chem.*, 2000, **67**, 122–127

[27]M. Kronelda S.Novikov, S. Saukko, P. Kuivalainen, P. Kostamo, V. Lantto, *Sensor. Actuat.*

*B- Chem.*, 2006, **118**, 110-114.

[28] Y. Zhao, Z. Feng, & Y. Liang, *Sensor. Actuat. B- Chem.*, 1999, **56**, 224-227.

[29] C. Bittencourt, E. Llobet, M.A.P. Silva, R. Landers, L. Nieto,K.O. Vicaro, J.E. Sueiras, J. Calderer, X. Correig, *Sensor. Actuat. B- Chem.*, 2003, **92**, 67-72.

[30] K. M. Li, Y. J. Li, M. Y. Lu, C. I. Kuo, L. J. Chen, *Adv. Funct. Mater.*, 2009, **19**, 2453-2456.

[31] G. X. Wang, J. S. Park, M. S. Parkb, X. L. Gou, *Sensor. Actuat. B- Chem.*, 2008, **131**, 313-317.

[32] J. Zhang, J. Guo, H. Y. Xu, and B. Q. Cao, *ACS Appl. Mater. Interfaces*, 2013, **5**, 7893-7898.

[33] R. Rella, A. Serra, P. Siciliano, L. Vasanelli, G. De, A. Licciulli, A Quirini, *Sensor. Actuat. B- Chem.*, 1997, **44**, 462-467.

[34] I. T. Weber, R. Andrade, E. R. Leite, E. Longo, *Sensor. Actuat. B- Chem.*, 2001, **72**, 180-183.

[35] J. Y. Zheng, S. I. Son, T. K. Van and Y. S. Kang, *RSC Adv.*, 2015, **5,** 36307-36314.

[36] F. Tsin, A. Venerosy, J. Vidal, S. Collin, J. Clatot, L. Lombez, M. Paire, S. Borensztajn, C. Broussillou and P. P. Grand, *Sci. Rep.*, 2015, **5,** 8961.

[37] Y. Q. Wang, T. T. Jiang, D. W. Meng, J. Yang, Y. C. Li, Q. Ma and J. Han, *Appl. Surf. Sci.*, 2014, **317,** 414-421.

[38] H. B. Kim, H. Kim, H. S. Sohn, I. Son, H. S. Lee, *Mater. Lett.,* 2013, **101,** 65-68.

[39] X. F. Song, L. Gao, and S. Mathur, *J. Phys. Chem. C,* 2011, **115**, 21730–21735.